RESEARCH ARTICLE

How to cite: Angew. Chem. Int. Ed. 2021, 60, 12001–12006
International Edition: doi.org/10.1002/anie.202100507

German Edition: doi.org/10.1002/ange.202100507

A multifunctional Dysprosium-carboxylato 2D metallorganic framework

Jonay González,[a] Pablo Sevilla,[b] Guillem Gabarró-Riera,[a,f] Jesús Jover,[a,c] Jorge Echeverría,[a,c] Sara Fuertes,[d] Ana Arauzo[e], Elena Bartolomé,*[b] E. Carolina Sañudo*[a,f]

[a] J. González, G. Gabarró-Riera, Dr. J. Jover, Dr. J. Echeverría, Dr. E. C. Sañudo
Secció de Química Inorgànica, Departament de Química Inorgànica i Orgànica, Universitat de Barcelona
C/Martí i Franquès, 1-11, 08028 Barcelona, Spain
E-mail: esanudo@ub.es
[b] Dr. P. Sevilla, Dr. E. Bartolomé
Department of Mechanical Engineering. Escola Universitària Salesiana de Sarrià (EUSS). Passeig de Sant Joan Bosco, 74, 08017, Barcelona, Spain
E-mail: ebartolome@euss.es
[c] Dr. J. Jover, Dr. J. Echeverría
Institut de Química Teòrica i Computacional, Universitat de Barcelona
08028, Barcelona, Spain
[d] Dr. Sara Fuertes
Departamento de Química Inorgánica, Facultad de Ciencias, Instituto de Síntesis Química y Catalisis, Homogénea (ISQCH), CSIC−Universidad de Zaragoza, Spain
[e] Dr. A. Arauzo
Instituto de Nanociencia y Materiales de Aragón (INMA), CSIC-Universidad de Zaragoza, Zaragoza 50009, Spain.
E-mail: arauzo@unizar.es
[f] G. Gabarró, Dr. E. C. Sañudo
Institut de Nanociència i Tecnologia, Universitat de Barcelona IN2UB
C/Martí i Franquès, 1-11, 08028 Barcelona, Spain

Supporting information for this article is given via a link at the end of the document.

Abstract: We report the microwave assisted synthesis of a bidimensional (2D) MOF of formula $[Dy(MeCOO)(PhCOO)_2]_n$ (**1**) and its magnetically diluted analogue $[La_{0.9}Dy_{0.1}(MeCOO)(PhCOO)_2]$ (**1d**). **1** is a 2D material with single-ion-magnet (SIM) behaviour and **1d** is a multifunctional, magnetic and luminescent 2D material. **1** can be exfoliated into stable nanosheets by sonication.

Introduction

The study of matter at the nanoscale has opened huge possibilities in technological advances towards faster, smaller and more energy-efficient technological devices. The development of 2D materials poses new challenges but also offers exciting possibilities for the study of physical phenomena and properties at the 2D limit. Current interest in 2D materials is concerned mainly with the possible application in ultrathin devices, catalysis, sensing[1] and magnetism.[2] Most well studied 2D materials are inorganic solids, or the very well-known graphene.[3] Advances in inorganic 2D materials have allowed the study of superconductivity at the 2D limit[4] or the layer-dependent ferromagnetism in Van der Waals crystals.[5] Inorganic 2D materials are used to exploit proximity effects on graphene, being magnetic 2D metal organic frameworks (MOFs) an alternative to the known 2D inorganic materials.[6]

The chemical control provided by coordination chemistry can be exploited in this area, making possible defect-free 2D nanosheets, to tune aggregation of the nanosheets, as shown by Choi and co-workers, by modifying the ligand in ways that do not affect the binding sites[7], to form 2D materials for planar qubits[8], or to provide multifunctional properties to the material by ligand functionalization, as is currently done for coordination complexes that combine multiple properties like magnetism and luminescence[9–15] or photochromism.[16,17]

There are already several examples of 2D MOFs, usually relying in polytopic planar ligands or molecules that afford a coordination network in two dimensions with suitable linkers.[18–20] In many cases, these 2D MOFs are formed of charged layers with the counter ions in the lamellar space[21], which makes them brittle and difficult to exfoliate. For exfoliation, neutral 2D MOFs, organized in three dimensions by weak Van der Waals (VdW) forces would be preferred. The non-covalent bonding between layers would allow the exfoliation without disturbing the bonding within the layer. Exfoliation of the bulk 2D MOF material into nanosheets is an important step for the use of these nanoobjects in devices or materials, and the most relevant techniques are reviewed in several papers.[22–24] For 2D MOFs formed of neutral VdW stacked nanosheets exfoliation by sonication in a liquid matrix should result in nanosheets stable towards aggregation, as observed for some 2D materials.[1,25] This last point is very relevant for further manipulation of the nanosheets, for surface deposition, or for the formation of multilayer heterostructures.

Among other groups, in our laboratory we have pioneered the use of microwave assisted synthesis in coordination chemistry.[26–32] Many groups have also used microwave assisted synthesis for the preparation of MOFs[33] due to the advantages of this technique: the very short reaction times and the isolation of a single, pure product.

Herein, we present a simple method for the microwave assisted synthesis of a 2D MOF formed by neutral nanosheets stacked into microcrystals by Van der Waals interactions and its structural, thermo-magnetic and optical characterization.

Experimental

All chemicals and solvents were purchased from comercial sources and used as received.

Synthesis of 1. 0.0883 g of hydrated $Dy(MeCOO)_3{\cdot}xH_2O$ (0.26 mmol) and 0.063 g of PhCOOH (0.52 mmol) were placed in a microwave reactor tube with 4 mL of a MeOH:MeCN mixture in 1:1 proportion. A pulse of 150 W is applied and the reaction kept for 10 minutes at a maximum temperature of 125ºC. The reaction is cooled to room temperature and a colorless precipitate is filtered off. The solution is left for 9 days at 40ºC; after this time

colorless crystals of $[Dy(MeCOO)(PhCOO)_2]_n$ were obtained in 29% yield. The precipitate is analyzed by infrared (IR) and powder X-ray diffraction (PXRD) and found to be the same material. Total yield: 35%. Elemental analyses calculated (experimental): C 41.43 (41.05)%; H 2.83 (2.92)%. IR data (cm^{-1}): 3069 (w), 3039 (w), 3023 (w), 1590 (s), 1536 (s), 1436 (w), 1394 (s), 1331 (s), 1248 (m), 1164 (s), 1068 (w), 1022 (w), 993 (m), 930 (m), 868 (w), 847 (w), 830 (w), 788 (m), 709 (s), 700 (s), 687(s), 667 (s), 617 (w), 604 (w).

Synthesis of 1d: The experimental procedure follows that of complex **1**, using a mixture of $La(MeCOO)_3 \cdot xH_2O$ and $Dy(MeCOO)_3 \cdot xH_2O$ in 9:1 molar ratio.

Exfoliation of 1. 1 mg of microcrystals of **1** were placed in 5 mL of i-propanol in a crystallization tube with a screw cap. The mixture was sonicated in a VWR sonicator bath at 45 kHz and 120 W for 1 hour at 30ºC. After this time the dispersion is centrifuged at 4500 rpm for 10 minutes and the colourless dispersion of nanosheets decanted from the remaining white solid. The clear dispersion produces the Tyndall effect as expected. At 24 hours and 2 weeks, samples of the dispersion are deposited onto TEM grids and observed by TEM showing the presence of isolated nanosheets and aggregates of only a few nanosheets (Figure S5).

Crystallography. X-Ray diffraction data for **1** were collected on a Bruker APEXII SMART diffractometer using Molybdenum K-alfa microfocus radiation source (lambda = 0.71073 Å). The structures were solved by Patterson or intrinsic phasing methods (SHELXS2013 and SHELXT) and refined on F^2 (SHELXL-2016). Hydrogen atoms were included on calculated positions, riding on their carrier atoms. Powder X-ray diffraction data for **1** (precipitate), **1** (crystals) and **1d** were collected at the *Centres Científics i Tecnològics- Universitat de Barcelona* (CCiTUB).

Thermogravimetric analyses and Diferential Scanning calorimetry. TGA and DSC analyses were performed at the Unitat de Polimorfisme i Calorimetria CCiTUB using a Star SW 16.10 analyser.

Emission studies. Solid state and solution luminescent measurements: Quantum yield (QY) was measured using a Hamamatsu Absolute PL Quantum Yield spectrometer C11347 (Hamamatsu Quantaurus QY). The absolute QY (ratio of the number of photons emitted by photoluminescence to the number of photons absorbed by the light-emitting material) was measured using an integrating sphere. Powdered samples were placed in a capillary with an internal diameter of 1 mm. Solution samples were placed in a standard quartz cell. The absorption and emission spectra of the sample container (the blank) were separately recorded. The QY was calculated as: $Q = (E_c - E_a)/(L_a - L_c)$ with E_c being the integrated emission spectrum of the sample, E_a the integrated blank emission spectrum, L_a the blank absorption, and L_c the sample adsorption at the excitation wavelength. Photoluminescence emission and excitation spectra were measured using a Fluorolog FL-1057 Jobin Ybon HORIBA spectrofluorometer. Phosphorescence lifetimes were recorded with a Fluoromax phosphorimeter accessory containing a UV xenon flash tube.

Microscopy. Transmission Electron Microscopy (TEM) were performed at CCiTUB. Specimens were analyzed using a JEOL JEM-2100 LaB6 transmission electron microscope with energy dispersed analysis of X-Rays (EDX), operating at 200 kV. The spectrometer is an Oxford Instruments INCA x-sight, with Si (Li) detector; acquisition was accomplished using the INCA Microanalysis Suite version 4.09 software. Images were recorded with Gatan CCD Camera Orius SC1000 and Digital Micrograph v.1.82.80 software. Scanning Electron Microscopy (SEM) were performed at CCiTUB. Specimens were coated in graphite and analyzed on the CCiTUB facilities, atomic force microscopy (AFM) was measured at CCiT UB Unit Tècniques Nanomètriques with a Multi mode AFM. The electronics of the system are Nanoscope V from Bruker. Topographic mode: peak force using "ScanAssist". Each image has a resolution of 512x512 pixels, taken at a velocity of 1 row/s. Tip used: silicon oxide with a nominal radius of 5 nm.

Thermo-magnetic measurements. Thermo-magnetic measurements were performed at *Servicio de Medidas Físicas-SAI (Universidad de Zaragoza)*. Dc magnetometry and ac susceptibility measurements were collected from powdered samples, embedded in n-hexane to avoid grain orientation. Dc measurements ($M(H)$ at T=1.8 K, from H=0-50 kOe and $\chi(T)$ from 1.8 to 300 K, at an applied field of 1 kOe) and ac susceptibility measurements (χ', $\chi''(f, H, T)$, at fields between H=0-30 kOe, T=1.8-8 K, at an excitation field of H_{ac}=4 Oe in the frequency range f=0.1-1000 Hz) were performed in a Quantum Design magnetometer. Additional ac susceptibility measurements in the frequency range between f=100-10^4 Hz were carried on in a Quantum Design PPMS. Heat capacity under different applied fields (0 - 30 kOe) was measured down to 0.35 K on a pressed powder pellet fixed with Apiezon N grease, using the same PPMS equipped with a ^{3}He refrigerator.

Results and Discussion

Crystal structure of $[DyMeCOO)(PhCOO)_2]$ (**1**) is determined by single-crystal X-ray diffraction. The crystallographic parameters are summarized in Table S1. Observation of the precipitate and of the crystalline sample by scanning electron microscopy (SEM) shows that both the precipitate and the crystals are mainly formed of plate-like microcrystals. The precipitate shows more polydispersity on the size of the platelets, but for the crystalline sample the average size is 2.5x30x40 micrometers, as shown in Figure 1a. All the samples observed are homogeneous and microplates thicker than 3 μm are rare. The electron dispersive x-ray analyses (EDS) of both the precipitate and the crystals confirm the presence of Dy (for more SEM images see ESI Figure S1).

The crystal structure of **1** consists of Van der Waals stacked nanosheets of a simple 2D MOF of formula $[Dy(MeCOO)(PhCOO)_2]_n$ (**1**). The Dy center has coordination number 8 (Figure 1b), and the coordination polyhedra according to SHAPE is between a very distorted square antiprism and a biaugmented trigonal prism (see ESI Table S2). The acetato ligand is in a *chelate, anti, anti*-acetato binding mode, bridging three dysprosium ions. All the benzoato ligands are in the common *syn,syn*-benzoato bridging mode and bridge two dysprosium ions. Nanosheets are stacked along the *a* direction of the unit cell and are 1.6 nm thick, thus a microcrystal of 1 μm is formed of approx. 625 nanosheets. There is no crystallization solvent that separates the nanosheets, Van der Waals interactions between nanosheets extend along the *bc* plane of the unit cell (Figure 1c). Each nanosheet can be described as a corrugated array of hexagonal tiles, with the Dy ions placed in the vertexes (Figure 1d). The phenyl groups of the benzoate ligands form a hydrophobic layer on top and below the acetate-Dy corrugated layer shown in Figure 1c. The nanosheets are neutral and hydrophobic. Su and coworkers reported in 2012 a 2D lanthanide-organic framework with a benzotriazole derivative and Ln = Eu, Sm, Gd and Tb.[34] The structure is similar to our compound **1** with a terminal H_2O ligand coordinated to the Ln ion and instead of the chelating, *anti,anti*-acetato coordination mode in complex **1**. This results in a different array of lanthanide ions in the 2D plane and will be relevant for the magnetic properties of **1**. Furthermore, the benzotriazole groups allow for N-H--N hydrogen bonding between 2D layers in Su's compounds, so that the

interaction between layers is much stronger than the pure Van der Waals interactions in the present compound **1**.

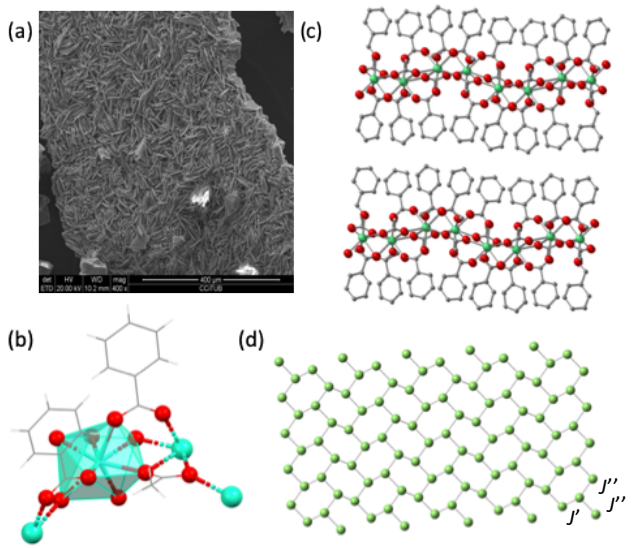

Figure 1. (a) SEM image of a sample of **1** obtained after 1 week at 40ºC, (b) Detail of Dy coordination environment for **1**. (c) Crystal packing view along the *bc* plane of the unit cell, showing stacking of the nanosheets along the *a* axis of the unit cell for **1** (hydrogen atoms omitted for clarity). (d) Topological arrangement of the Dy ions in the bc plane of the unit cell. Carbon: grey; Oxygen: red; Hydrogen: white; Dysprosium: green. The in-plane Dy-Dy interaction constants are indicated.

Powder X-ray diffraction pattern of a part of the same bulk microcrystalline sample observed by SEM coincides perfectly with the PXRD pattern simulated using the single crystal X-ray diffraction structure (see ESI Figure S2), confirming that the bulk material is formed of microcrystals of the same Van der Waals stacked nanosheets. An isostructural magnetically diluted compound, $[La_{0.83}Dy_{0.17}(MeCOO)(PhCOO)_2]$ (**1d**), was also prepared. SEM images of the crystals of **1d** show plate-like crystals and EDS analysis on the SEM microscope confirms the presence of La and Dy (Figure S1). PXRD of **1d** confirms it is isostructural to **1** (Figure S2).

Thermogravimetric analysis (TGA) and differential scanning calorimetry (DSC) of compound **1** show that the compound melts at 244ºC. After melting the compound decomposes with two main events at 384ºC and 556ºC. Weight loss analyzed by TGA is in agreement with the loss of most of the phenyl groups at 384ºC (20% mass lost, over the 33% that the phenyl groups represent on the total mass of the sample) and the total loss of the organic matter at 556ºC to form dysprosium oxide (49% of the total mass left at 600ºC) (see Figure S3). To evaluate the porosity of the material, gas sorption isotherm was measured. The sorption and desorption of N_2 revealed a Type II isotherm with type H3 hysteresis, according to IUPAC classification. This is typical of nonporous or macroporous materials, formed of non-rigid aggregates of plate-like particles (see Figure S4).[35,36] BET surface area for **1** is 3.5 m^2/g, a low value that is in agreement with the layered structure of **1**.

Static magnetic measurements of powdered complexes **1**, **1d** are shown in Figure 2a. The magnetization vs. magnetic field curves, $M(H)$, measured at T=1.8 K reach the value of 5 μ_B at 50 kOe expected for a random distribution of Dy^{3+} ($^6H_{15/2}$) ions. The $M(H)$ of **1d** is perfectly fit by a model of non-interacting Dy ions with the g^*-values calculated by *ab initio* and a small van Vleck contribution. The magnetic susceptibility was investigated under 1 kOe in the range of 1.8-300 K and is shown as a $\chi T(T)$ plot in Figure 2a. The χT value at 300 K for **1**, **1d** (13.7 emu K/mol) is slightly below the expected free-ion Ln^{3+} value. Upon cooling, χT decreases with T and reaches 9.6 emu.K/mol at 1.8 K for **1d**, while for **1**, χT decreases to a minimum value of 9.4 emu.K/mol at 2.4 K but then increases again reaching 9.9 emu.K/mol at 1.8 K (Fig. 2a, inset). The Curie-Weiss equation, χ=C/(T-θ), was used to fit the $1/\chi(T)$ data, giving C=13.97 emu.K/mol, $\theta = -4.8$ K for **1**. The negative θ value is indicative of the existence of predominant antiferromagnetic (AF) dipolar-dipolar interactions between the Dy ions, while the χT upturn feature observed upon cooling, absent in the diluted compound, points to the existence of ferromagnetic (FM) interactions between nearest-neighbor Dy ions, competing at low temperatures.

The heat capacity as a function of the temperature at different fields was measured for **1** (Figure 2b). The magnetic contribution at H=0, after subtracting the lattice contribution, $C_m(T)$, exhibits a sharp peak at T_N=0.85 K. The entropy $S(T)$ and internal energy $U(T)$ dependencies were determined from the experimental $C_m(T,H=0)$ data,[37] and the critical entropy and energy were found to be S_c/R=0.394 and $-U_c/T_c$=0.509, respectively. These values are intermediate between the theoretically predicted values for a 2D honeycomb ½-Ising model (S_c/R=0.2647 and $-U_c/T_c$=0.76) and those predicted for 3D ½-Ising models in any lattice configuration (e.g., for a s.c. lattice, S_c/R=0.5579 and $-U_c/T_c$=0.22).[38] Thus, complex **1** magnetically behaves as a 2D honeycomb at $T>T_N$, with some interlayer interaction, that allows upon cooling the establishment of an AF 3D long-range ordering at T_N=0.85 K. The heat capacity at $T<T_N$ follows a power-law dependence $T^{d/n}$ with d/n≈3, which confirms the AF-3D nature of the ordering, according to Kubo's theory. The magnitude of the average intralayer Dy-Dy interactions can be estimated from the value of T_N under the 2D honeycomb ½-Ising model, which predicts[37] $k_B T_N / |J| = 0.379663$, yielding $|J| / k_B = 2.24$ K (expressed in the effective spin S^*=1/2 coupling Hamiltonian $H = -J\sum_{i,j} S_i^* S_j^*$).

The electronic structure of **1** was computed with the *ab initio* CASSCF method for a polynuclear Dy-La-Y (ESI Figure S9) complex directly extracted from the crystal structure. The components of the gyromagnetic tensor, $\hat{g}^*$, calculated within a S^*=1/2 ground state description (g_x^* = 0.007, g_y^* = 0.020, and g_z^* = 19.281), indicate a strong anisotropic character for the Dy single-ion. The *ab initio* computed easy axes of magnetization (EAM) of the Dy(III) ions are tilted away from the Dy-acetato plane, and the axes of nearest neighbor (n.n.) Dy centers are parallel (Figure S10). The anisotropy axes computed using the software Magellan[39] (where a very simple point charge model is used to find the main anisotropy axis) for a larger fragment containing 16 Dy ions from the Dy-acetato layer show a good agreement with those obtained by *ab initio*. The angle between the anisotropy axes calculated by Magellan and the axes calculated by *ab initio* is *ca.* 18º. The dipolar interactions between each Dy ion with its first neighbors were calculated, within the effective Hamiltonian, with the expression:

$$J_{dip} = \frac{\mu_0}{4\pi r^3}\left(3\cos\theta_1\cos\theta_2 - \cos\theta_{12}\right)\mu_B^2 g_z^{*2},$$

taking into account the separation r and relative orientation of the EAM of the considered Dy ions, known from *ab initio*. The obtained in-plane dipolar coupling constants were J'/k_B=-1.93 K and J''/k_B=-2.43 K, between the Dy-Dy ions in the irregular 2D honeycomb structure shown in Figure 1d. The calculated inter-plane dipolar coupling was an order of magnitude smaller, J'''/k_B=-0.11 K. (Very similar values were obtained using the EAM calculated with Magellan, J'/k_B=-1.98 K, J''/k_B=-2.27 K, J'''/k_B=-0.10 K). Since the average intraplane Dy-Dy interaction calculated from the heat capacity, encompassing both dipolar and

exchange contributions, $J = J_{ex} + J_{dip}$, was in module 2.24 K, it is deduced that part of this interaction must be of exchange nature. This is plausible, in view of the possible exchange pathways observed from the crystal structure of complex **1**. Each Dy ion the honeycomb has one nearest-neighbor at 3.906 Å and two at 4.675 Å. For the shortest distance, there are two monoatomic oxygen bridges from *chelating, anti, anti-* acetato ligands that link 3 Dy ion, which are very effective to facilitate magnetic exchange. For the longest distance, there is also one monoatomic oxygen bridge from the *chelating, anti, anti-* acetato ligand.

Alternating-current (ac) susceptibility measurements as a function of frequency (0.1-10 kHz), temperature (T = 1.8 - 8 K) and field (H = 0-30 kOe) were performed to explore the dynamics of the magnetization of **1** and **1d** in powder form. Complex **1** did not show frequency dependent out-of-phase χ'' signal under H=0. Upon application of a dc field, quantum tunneling of the magnetization (QTM) was effectively suppressed and slow relaxation of the magnetization effects were observed. The χ''(f, T) curves at optimum field H = 2 kOe, and χ''(f, H) data at T=2 K are shown in Figs. 2c-2d. From the position of the χ'' peaks, the relaxation time as a function of the inverse temperature and the magnetic field were determined (Figs. 2e-2f). The occurrence of multiple relaxation channels is observed. The intense peak χ'' measured at low frequencies shows relaxation time dependencies, $\tau_{LF}(1/T)$ and $\tau_{LF}(H)$, typical of a direct process mechanism affected by phonon bottleneck. At higher frequencies and under the application of a dc field, a second intense peak χ'' is observed, associated to a thermally-activated process that affords an Arrhenius law for the relaxation time, $\tau_{TAQT} = \tau_0.\exp(U/k_BT)$, with U/k_B=15.3 K and τ_0=1,0x10^{-5} s, in the range 5-8 K. Upon decrease of the temperature this process is replaced by QTM, as evident from the flat $\tau(1/T)$ dependence between 3-5 K. By further decreasing the temperature, the high frequency χ'' maximum broadens, and is possible to discriminate multiple peaks at certain (H,T) conditions, from which the $\tau_{HF}(1/T)$ and $\tau_{HF}(H)$ data shown in Figs. 2e-2f were obtained. This behavior points to the existence of multiple tunneling relaxation channels via different energy levels close in energy, with relaxation times in a range between τ_{HF}~1.6x10^{-5}-8.0x10^{-4} s (grey band in the figure). This complex relaxational phenomena may be triggered by the existence of multiple interactions of different hierarchy between Dy ions (exchange, FM interactions, versus AF intralayer and interlayer dipolar interactions), competing at low temperatures, in agreement with $\chi T(T)$ evidence. In the absence of interactions, the diluted complex **1d** displays single-ion magnet (SIM) behavior even under H=0 Oe (Figs. 2e-2f). *Ab initio* calculations of the Dy single-ion dynamics confirm the existence of different channels of fast relaxation between the lowest four Kramer's doublets (Figure S11), which become effective in virtue of Dy interactions.

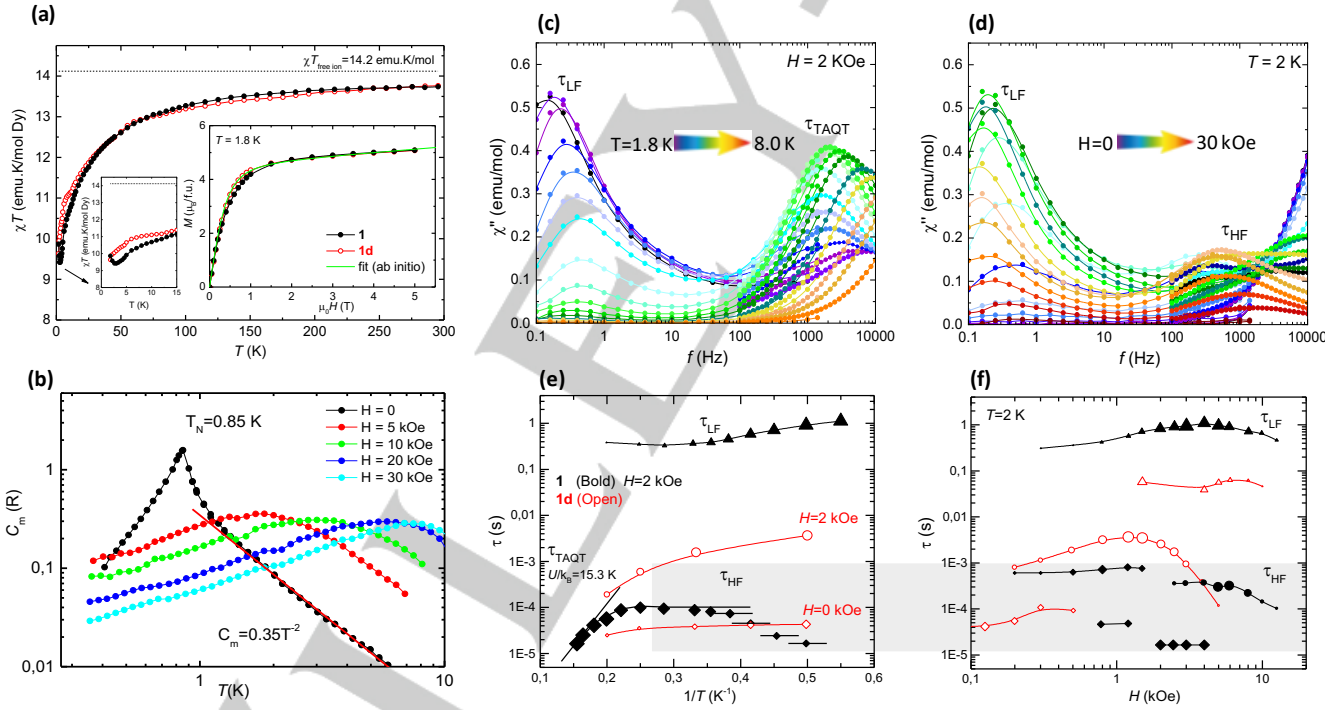

Figure 2. (a) Temperature-dependence of the product χT at 1 kOe, and Inset: field-dependence of the magnetization at T=1.8 K, for complexes **1** and **1d**. (b) Magnetic contribution to the heat capacity as a function of the temperature at different fields for **1**. (c-d) Out-of-phase component of the susceptibility as a function of frequency for compound **1**, (c) at different temperatures from T = 1.8 K to 8.0 K at constant applied field, H = 2 kOe, (d) at different fields from 0-30 kOe, at T = 2 K. (Data for **1d** are in Fig. S3). (e) Relaxation time of the different processes observed as a function of the inverse of the temperature, and (f) as a function of field for compounds **1** and **1d**.

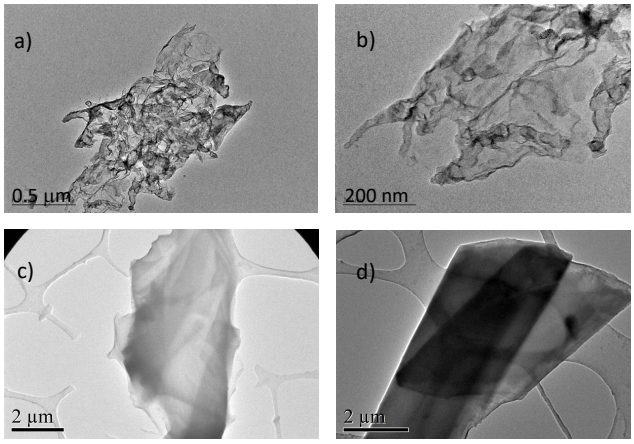

Figure 3. TEM images on a carbon Cu grid (a and b) and a lacey carbon Cu grid (c and d) of **1** nanosheets deposited from isopropanol. Images (a) and (b) were obtained one week after exfoliation, images (c) and (d) where obtained three weeks after exfoliation.

The nanosheets of **1** can be exfoliated in isopropanol by sonication at 30ºC for 1 hour. Centrifugation for 10 minutes at 4500 rpm ensures the removal of microcrystals. Sonication for shorter periods of time results in similar exfoliation but more multilayer objects are observed in TEM, even after centrifugation. The Tyndall effect can be observed in the isopropanol suspension of 2D nanosheets of **1** (ESI Figure S7). Deposition on a TEM grid allows observation of single or multiple nanosheets that upon EDS analysis show the right composition (Dy, C and O, Figure S7). The nanosheets are stable in iPrOH for at least three weeks (Figure 3 and ESI Figure S7). This material is composed of neutral 2D layers that offer a surface of vertically oriented phenyl groups: the interaction between layers are thus weak Van der Waals interactions. We have calculated an interaction energy of -113 kJ/mol for two interacting monolayers of the size of a unit cell. For comparison, the interaction energies of two-layer graphene and graphane (with the same surface size as our 2D MOF) are -274 and -97 kJ/mol, respectively.

The nanosheets seem to fold upon themselves on the TEM grid (carbon or lacey carbon Cu grids), as shown in Figure 3. This is not unusual for similar neutral 2D materials like graphene.[40] Clearly stabilization of the nanosheets is one important challenge we face for the possible use of single layers of compound **1**. Delamination or exfoliation conditions for a neutral 2D MOF have been reviewed by Coronado *et al* in a recent communication where the authors achieve regularly shaped flakes of large lateral size and thickness of 3-4 layers.[24]

Atomic Force Microscopy images (AFM) can be obtained from drop casted and spin coated dispersions of exfoliated nanosheets in various substrates. Figure 4 shows AFM images of two single flakes on thermally oxidized silicon wafer spin coated at 500 rpm for 60 s and at 1000 rpm for 45 s. More images can be found in ESI material Figure S8. We have used mica, HOPG and silicon wafers with thermal SiO_2 layers (Figure S8). In all substrates flakes of various sizes and heights of circa. 2 nm were observed. The observed heights are consistent with single nanosheets of compound **1** on the surface. In some cases, stacks of several nanosheets and larger nanocrystals can be observed, in particular for HOPG since nanosheets accumulate in the terraces of the material (Figure S8). Further efforts will be directed to the optimization of the exfoliation process and the stabilization of monolayers of **1**.

Photoluminescent measurements in the solid state showed the Dysprosium 2D-MOF material **1** is not luminescent. However, the diluted species **1d** displayed the emission spectra for Dy(III) when excited at 280 nm. We confirm thus the antenna effect from the benzoato ligands. The quantum yield of the emission was relatively high for a Dy complex (QY = 4%),[41,42] and the luminescent lifetime was 50 μs (Figure 5). It is concluded that high concentration of Dy(III) centers in **1** quenches the luminescence. Once the Dy(III) ions are isolated in **1d**, luminescence can be observed.

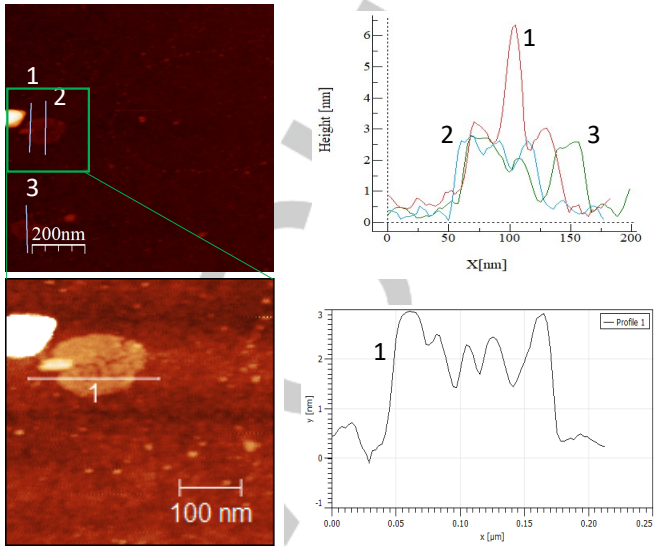

Figure 4. AFM image of a thermally oxidized Si wafer on which two drops of exfoliated **1** in i-PrOH have been deposited by spin coating.

The magnetically diluted sample **1d** was exfoliated in isopropanol following the same procedure used for compound **1**. The small amount of Dy present in the sample is reflected in the low intensity of the emission. However, clearly one can identify the emission from Dy (Figure 5), as seen in the solid state experiment.

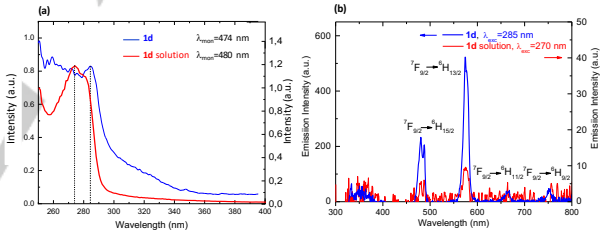

Figure 5. Photoluminescence results for complex **1d** in solid state and in exfoliated form in solution; (a) Excitation spectra, (b) emission spectra after excitation. The QY = 4% of 1d in the solid state was obtained by integration of the emission in the 460 – 800 nm range.

Conclusions

In summary, we have presented an extremely simple synthesis method for the preparation of a Dy-based 2D MOF displaying SIM behaviour. In the magnetically diluted Dy compound, the quenching of the magnetic interactions allows the observation of simultaneously single-ion slow relaxation of the magnetization and luminescence emission in the visible. This is, to the best of our knowledge, the first case of a bifunctional 2D luminescent SMM. The method is being applied in our laboratories to synthesize different lanthanide 2D MOFs, and heterogeneous Ln-Ln' 2D MOFs with tunable color emission. Our findings enable an effective, robust approach to develop multifunctional 2D MOFs for different applications. The facile exfoliation of **1** into stable nanosheets is very promising for further manipulation of the material, for deposition onto different surfaces, to exploit proximity effects on graphene, or the formation of multilayer hetero-nanostructures.

Acknowledgements

We acknowledge financial support by the Spanish Ministry of Science and Innovation through PGC2018-098630-B-I00 (ECS), PGC2018-093863-B-C21 and DWARFS (MAT2017-83468-R) (EB, AA) and PGC2018-094749-B-I00 (SF) projects. JJ and JE acknowledge the MDM-2017–0767 grant from the Spanish Structures of Excellence María de Maeztu program. Authors acknowledge the help of Joan Mendoza (CCiTUB TEM-Mat) for obtention of TEM images.

Keywords: 2D materials · Van der Waals interactions · Lanthanides · Magnetic properties ·Lluminescence

References

[1] F. Moghzi, J. Soleimannejad, E. C. Sañudo, J. Janczak, *ACS Appl. Mater. Interfaces* **2020**, *12*, 44499–44507.

[2] E. Coronado, *Nat. Rev. Mater.* **2020**, *5*, 87–104.

[3] P. MIró, M. Audiffred, T. Heine, *Chem. Soc. Rev.* **2014**, *43*, 6537–6554.

[4] E. Navarro-Moratalla, J. O. Island, S. Manãs-Valero, E. Pinilla-Cienfuegos, A. Castellanos-Gomez, J. Quereda, G. Rubio-Bollinger, L. Chirolli, J. A. Silva-Guillén, N. Agraït, et al., *Nat. Commun.* **2016**, *7*, 1–7.

[5] B. Huang, G. Clark, E. Navarro-Moratalla, D. R. Klein, R. Cheng, K. L. Seyler, Di. Zhong, E. Schmidgall, M. A. McGuire, D. H. Cobden, et al., *Nature* **2017**, *546*, 270–273.

[6] L. A. Benítez, J. F. Sierra, W. Savero Torres, A. Arrighi, F. Bonell, M. V. Costache, S. O. Valenzuela, *Nat. Phys.* **2018**, *14*, 303–308.

[7] S. Yang, S. Kang, T. Choi, *J. Am. Chem. Soc.* **2019**, *141*, 19138–19143.

[8] A. Urtizberea, E. Natividad, P. J. Alonso, M. A. Andrés, I. Gascón, M. Goldmann, O. Roubeau, *Adv. Funct. Mater.* **2018**, *28*, 1–15.

[9] S. Gholizadeh Dogaheh, H. Khanmohammadi, E. C. Sañudo, *New J. Chem.* **2017**, *41*, 10101–10111.

[10] M. Menelaou, F. Ouharrou, L. Rodríguez, O. Roubeau, S. J. Teat, N. Aliaga-Alcalde, *Chemistry* **2012**, *18*, 11545–11549.

[11] K. Soussi, J. Jung, F. Pointillart, B. Le Guennic, B. Lefeuvre, S. Golhen, O. Cador, Y. Guyot, O. Maury, L. Ouahab, *Inorg. Chem. Front.* **2015**, *2*, 1105–1117.

[12] F. Pointillart, B. Le Guennic, T. Cauchy, S. Golhen, O. Cador, O. Maury, L. Ouahab, *Inorg. Chem.* **2013**, *52*, 5978–5990.

[13] R. Marin, G. Brunet, M. Murugesu, *Angew. Chemie Int. Ed.* **2019**, DOI 10.1002/anie.201910299.

[14] J. H. Jia, Q. W. Li, Y. C. Chen, J. L. Liu, M. L. Tong, *Coord. Chem. Rev.* **2019**, *378*, 365–381.

[15] S. Benmansour, A. Hernández-Paredes, A. Mondal, G. López Martínez, J. Canet-Ferrer, S. Konar, C. J. Gómez-García, *Chem. Commun.* **2020**, *56*, 9862–9865.

[16] J. Salinas Uber, M. Estrader, C. Mathonière, R. Clérac, O. Roubeau, G. Aromí, *Cryst. Growth Des.* **2016**, acs.cgd.6b00556.

[17] M. Estrader, J. Salinas Uber, L. A. Barrios, J. Garcia, P. Lloyd-Williams, O. Roubeau, S. J. Teat, G. Aromí, *Angew. Chemie - Int. Ed.* **2017**, *56*, 15622–15627.

[18] M. Zhao, Y. Huang, Y. Peng, Z. Huang, Q. Ma, H. Zhang, *Chem. Soc. Rev.* **2018**, *47*, 6267–6295.

[19] D. D. Yin, Q. Chen, Y. S. Meng, H. L. Sun, Y. Q. Zhang, S. Gao, *Chem. Sci.* **2015**, *6*, 3095–3101.

[20] C. M. Liu, M. Xiong, D. Q. Zhang, M. Du, D. Ben Zhu, *Dalt. Trans.* **2009**, 5666–5672.

[21] J. López-Cabrelles, S. Mañas-Valero, I. J. Vitórica-Yrezábal, P. J. Bereciartua, J. A. Rodríguez-Velamazán, J. C. Waerenborgh, B. J. C. Vieira, D. Davidovikj, P. G. Steeneken, H. S. J. van der Zant, et al., *Nat. Chem.* **2018**, *10*, 1001–1007.

[22] D. J. Ashworth, J. A. Foster, *J. Mater. Chem. A* **2018**, *6*, 16292–16307.

[23] R. Sakamoto, K. Takada, X. Sun, T. Pal, T. Tsukamoto, E. Jia, H. Phua, A. Rapakousiou, K. Hoshiko, H. Nishihara, *Coord. Chem. Rev.* **2016**, *320–321*, 118–128.

[24] L. León-Alcaide, J. López-Cabrelles, G. Mínguez Espallargas, E. Coronado, *Chem. Commun.* **2020**, *56*, 7657–7660.

[25] G. A. Bhat, S. Haldar, S. Verma, D. Chakraborty, R. Vaidhyanathan, R. Murugavel, *Angew. Chemie - Int. Ed.* **2019**, *58*, 16844–16849.

[26] A. Pons-Balagué, S. Piligkos, S. J. Teat, J. Sánchez Costa, M. Shiddiq, S. Hill, G. R. Castro, P. Ferrer-Escorihuela, E. C. Sañudo, *Chem. Eur. J.* **2013**, *19*, 9064–9071.

[27] R. Díaz-Torres, M. Menelaou, O. Roubeau, A. Sorrenti, G. Brandariz-De-Pedro, E. C. Sañudo, S. J. Teat, J. Fraxedas, E. Ruiz, N. Aliaga-Alcalde, *Chem. Sci.* **2016**, *7*, 2793–2803.

[28] M. Ledezma-Gairaud, L. W. Pineda, G. Aromí, E. C. Sañudo, *Inorganica Chim. Acta* **2015**, *434*, 215–220.

[29] L. Rosado Piquer, E. C. Sañudo, *Polyhedron* **2019**, *169*, 195–201.

[30] A. Pons-Balague, N. Ioanidis, W. Wernsdorfer, A. Yamaguchi, E. C. Sanudo, *Dalt. Trans.* **2011**, *40*, 11765–11769.

[31] I. a Gass, C. J. Milios, a G. Whittaker, F. P. a Fabiani, S. Parsons, M. Murrie, S. P. Perlepes, E. K. Brechin, *Inorg. Chem.* **2006**, *45*, 5281–3.

[32] C. J. Milios, A. Vinslava, a G. Whittaker, S. Parsons, W. Wernsdorfer, G. Christou, S. P. Perlepes, E. K. Brechin, *Inorg. Chem.* **2006**, *45*, 5272–4.

[33] J. Klinowski, F. a A. Paz, P. Silva, J. Rocha, *Dalton Trans.* **2011**, *40*, 321–30.

[34] Z. H. Li, L. P. Xue, B. T. Zhao, J. Kan, W. P. Su, *CrystEngComm* **2012**, *14*, 8485–8491.

[35] K. A. Cychosz, R. Guillet-Nicolas, J. García-Martínez, M. Thommes, *Chem. Soc. Rev.* **2017**, *46*, 389–414.

[36] M. Thommes, K. Kaneko, A. V. Neimark, J. P. Olivier, F. Rodriguez-Reinoso, J. Rouquerol, K. S. W. Sing, *Pure Appl. Chem.* **2015**, *87*, 1051–1069.

[37] J. Strečka, M. Jaščur, *Acta Phys. Slovaca* **2015**, *65*, 235–367.

[38] R. Navarro, in *Magn. Prop. Layer. Transit. Met. Compd.* (Ed.: De Jongh), **n.d.**

[39] N. F. Chilton, D. Collison, E. J. L. McInnes, R. E. P. Winpenny, A. Soncini, *Nat. Commun.* **2013**, *4*, 2551.

[40] M. Haditale, R. S. Dariani, E. Ghasemian Lemraski, *J. Theor. Appl. Phys.* **2019**, *13*, 351–356.

[41] N. Wartenberg, O. Raccurt, E. Bourgeat-Lami, D. Imbert, M. Mazzanti, *Chem. a Eur. J.* **2013**, *19*, 3477.

[42] A. A. Kitos, D. A. Gálico, R. Castañeda, J. S. Ovens, M. Murugesu, *Inorg. Chem.* **2020**, *59*, 11061.

Entry for the Table of Contents

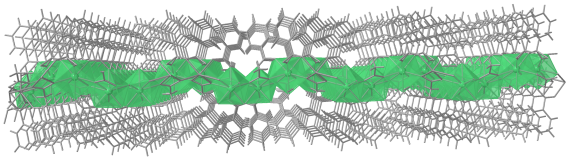

Microwave assisted synthesis is applied to prepare a Dysprosium 2D-MOF with simple carboxylato ligands, $[Dy(MeCOO)(PhCOO)_2]_n$ (**1**). The Dy(3+) ions are arranged in an hexagonal pattern into nanosheets, stacked by Van der Waals forces similar to those of graphene. The magnetically diluted MOF **1d** is a bifunctional 2D luminescent material with SMM properties.